MORPHOMETRY AND TIMING OF MAJOR CRUSTAL SHORTENING STRUCTURES ON MARS.

Rachel M. Atkins[1], Paul K. Byrne[1], Karl W. Wegmann[1], [1]Planetary Research Group, Department of Marine, Earth, and Atmospheric Sciences, North Carolina State University, Raleigh, NC 27695, USA (ratkins@ncsu.edu).

Introduction: The surface of Mars features a large population of structures attesting to widespread contractional and extensional stresses [1,2]. Crustal shortening is generally accommodated by low-angle thrust faults within the lithosphere that are manifest on the surface as a positive-relief landform with a steep scarp face and a gently sloping backscarp [3]. These structures range from tens to hundreds of km in length with hundreds to thousands of meters of relief [4]. The global distribution of these shortening structures has been attributed to their formation via the global contraction of Mars from secular cooling [5]. Measured offsets along these faults collectively yield calculations of a global radius decrease of 0.1–2.2 km [5].

Based on observations of thrust faults on Earth [6,7], lobate scarps on Mars are likely fault-propagation anticlinal folds that form in proportion to the accumulation of slip along the underlying fault, with maximum displacement for an isolated thrust fault at the center of the fold and decreasing to zero at the tips [3]. Through characterizing the morphology of the scarp and variations along its length, a history of fault growth and the extent of interactions with other faults can be obtained [8].

Notably, in many instances these lobate scarps are superposed by channel networks [3]. Further, in at least some cases, these channel networks are oriented downslope, supporting the possibility that the scarp was in place prior to, and thus influenced the formation of, the superposing channel. The acquisition of model ages via crater statistics can therefore provide first-order estimates of when large-scale crustal shortening took place—a major unknown for Martian tectonic and thermal history [5]. In this study, we assess a subset of lobate scarps on Mars and describe their morphological properties and growth histories, before using crater statistics to estimate their timing of formation.

Methods: We carried out a global survey and identified 33 lobate scarps as candidates for this study by analysis of the HRSC–MOLA blended digital elevation model (DEM) (spatial resolution ~200 m/px) and the THEMIS thermal image data set (100 m/px) in ESRI ArcGIS®. Scarps were selected for detailed study on the basis of their being relatively undisturbed by impact craters and showing little evidence for mechanical interaction with neighboring structures; as geographically distributed a set of structure as possible was chosen (**Figure 1**). Out of the 33 selected faults, ten have superposed channel networks that we investigate for our timing analysis.

The surface break of each structure was digitized with the Editor functions in ArcGIS and exported for use in MATLAB®, where transects were drawn perpendicular to each fault trace at 1 km spacing. This spacing represents an increase in detail of an order of magnitude compared with previous studies [e.g., 3]. From each transect the minimum and maximum relief of the scarp was identified, which in turn yielded throw values along the fault under the assumption that the relief of the landform corresponds to the vertical component of fault displacement.

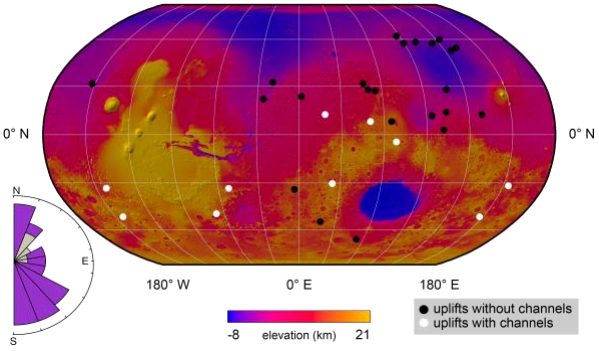

Figure 1. *Global distribution of Martian lobate scarps. Study fault systems shown with circles. Rose diagram (lower left) indicates overall N–S trend to the strike orientation of mapped uplifts.*

Measured throw values were plotted against fault length to produce displacement profiles (**Figure 2a inset**), which were then appraised for evidence of fault segmentation and linkage. The maximum throw values for each landform were plotted against their length values to determine maximum displacement (D_{max})-to-length (L) scaling ratio for each structure, and for the overall data set.

A modified hydrologic flow analysis using a "filled" DEM was performed in ArcGIS® using the Hydrology toolbox to indicate present-day downslope direction. These modeled channels were compared with the channels visible in THEMIS data. Co-alignment of visible channel segments and present-day downhill direction provides supporting evidence that channels formed in this orientation as the scarps already existed.

Craters on the scarp backlimbs (i.e., the hanging walls) were mapped with the CraterTools 2.1 plug-in for ArcGIS®. A minimum crater diameter threshold of 3 km was used to minimize the prospect of contamination of our crater statistics by secondary craters [9].

As determined by superposition and cross-cutting relationships, craters were grouped based on whether they pre- or post-date the channels. That is, craters with rims breached by channel segments, or that dramatically deflect the channel, were interpreted as pre-dating the channels, whereas craters (or their ejecta deposits) that superpose channels were taken as having formed following channel formation. For those craters not in direct contact with the channels, their morphological degradation states were compared with those that pre- or post-date the channels, and then classified as one of these two categories. Surface ages were calculated using Craterstats 2.0 [10] for the different crater populations to place model age estimates on the uplifted channel networks using the production function from Ivanov (2001) [11] and the chronology function from Hartmann and Neukum (2001) [12].

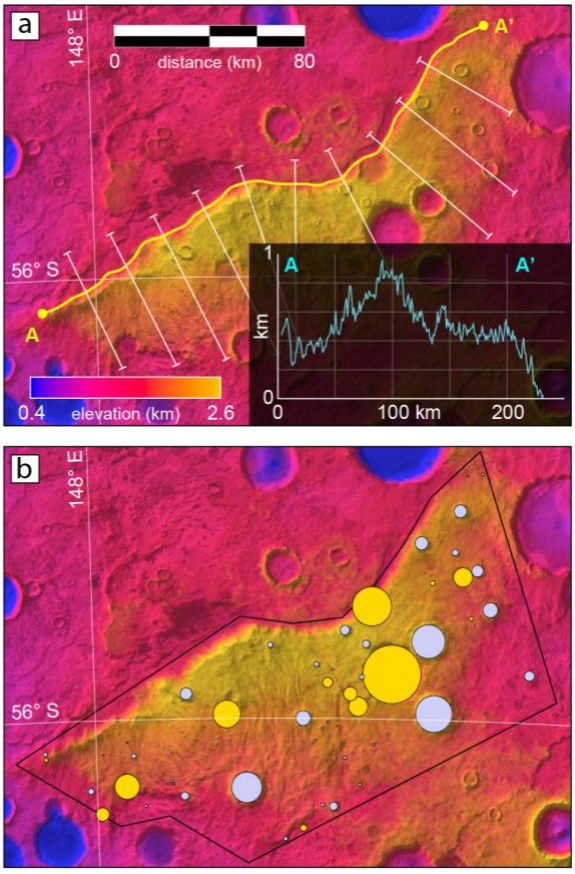

Figure 2. *Example uplift a) Leading edge of scarp mapped in yellow, with example transect lines in white; inset: displacement profile. b) Crater mapping results with those that predate channels in yellow, and those that postdate in lavender.*

Findings: The lobate scarps we investigate range in length from 36 to 623 kilometers, with fault strikes primarily trending N–S (**Figure 1 inset**). From 15 displacement profiles, maximum displacement values range from 86 to 2050 meters and have an overall D_{max}/L scaling ratio of 3.2×10^{-3}. This ratio falls within the range of calculated D_{max}/L values for Martian thrust faults: 2×10^{-3} to 7.5×10^{-3} [13, 14]. The inset in **Figure 2** shows evidence for growth of this structure largely in isolation since its displacement profile is peaked. However, maximum displacement is skewed slightly to the southwestern end of the structure, suggesting that at some point during growth the fault linked with a neighboring fault to the northeast.

In **Figure 2b**, we show mapped crater populations for a single scarp (**Figure 2b**). Craters cross-cut by, and thus older than, the channel network here are shown in yellow; those that show no evidence of being crossed by channels are shown in purple. We find a model age of 3.8 Ga for the pre-channel crater population and 3.7 Ga for that crater population formed after the channels were in place. (We do not quote formal errors for these age values.) These ages are not statistically different from each other, which leads us to conclude that this channel network formed very soon after the scarp had developed, with both being in place by the late Noachian/early Hesperian.

Outlook: The results we report here indicate that our globally distributed, large-scale Martian thrust faults have a D_{max}/L scaling relationship similar to other thrust fault populations. Continued detailed structural analyses of Martian thrust faults will provide greater insight into the morphology and growth histories of major crustal shortening structures on Mars. Moreover, model age dating utilizing crater–channel superposition relations will allow for the placing of tighter constraints on the timing of the global contraction and thus thermal evolution of the Red Planet.

References: [1] Hauck S. A. II and Phillips, R. J. (2002) *JGR, 107,* 1–19. [2] Solomon S. C. (1978) *Geophysical Research Letters, 5,* 461–464. [3] Klimczak C. et al. (2018) *JGR Planets, 123,* 1973–1995. [4] Knapmeyer M. et al. (2006). *JGR, 111,* 1–23. [5] Nahm A. L. and Schultz R. A. (2011) *Icarus, 211,* 389–400. [6] Suppe, J. and Medwedeff D. A. (1990) *Eclogae Geologicae Helvetiae,* 454, 409–454. [7] Wickham J. (1995) *Journal of Structural Geology, 17,* 1293–1302. [8] Cowie P. and Scholz C. (1992) *Journal of Structural Geology, 14,* 1149-1156. [9] Irwin R. P. et al. (2013) *JGR Planets, 118,* 278–291. [10] Michael G. and Neukum G. (2010) *Earth and Planetary Science Letters, 3,* 223-229. [11] Ivanov B. (2001) *Space Science Reviews, 96,* 87-104. [12] Hartmann W. and Neukum G. (2001) *Space Science Reviews, 96,* 165-194. [13] Watters T. (1988) *JGR Solid Earth, 93,* 10236-10254. [14] Schultz, R. et al. (2006) *Journal of Structural Geology, 28,* 2182-2193.